European Journal of Medicinal Chemistry 143 (2018) 390–401

Contents lists available at ScienceDirect

European Journal of Medicinal Chemistry

journal homepage: http://www.elsevier.com/locate/ejmech

Research paper

Design, synthesis, and biological evaluation of a series of resorcinol-based *N*-benzyl benzamide derivatives as potent Hsp90 inhibitors

Sun You Park [a, 1], Yong Jin Oh [a, 1], Yunmee Lho [b], Ju Hui Jeong [a], Kwang-Hyeon Liu [c], Jaeyoung Song [d], Soong-Hyun Kim [d], Eunyoung Ha [b, **], Young Ho Seo [a, *]

[a] College of Pharmacy, Keimyung University, Daegu 704-701, South Korea
[b] Department of Biochemistry, School of Medicine, Keimyung University, Daegu 704-701, South Korea
[c] BK21 Plus KNU Multi-Omics based Creative Drug Research Team, College of Pharmacy and Research Institute of Pharmaceutical Sciences, Kyungpook National University, Daegu 41566, South Korea
[d] New Drug Development Center, Daegu-Gyeongbuk Medical Innovation Foundation, Daegu 41061, South Korea

ARTICLE INFO

Article history:
Received 5 September 2017
Received in revised form
19 October 2017
Accepted 20 November 2017
Available online 21 November 2017

Keywords:
Hsp90 inhibitor
Lung cancer
Resistance
Small molecule
Drug design

ABSTRACT

Heat shock protein 90 (Hsp90) is a ubiquitous molecular chaperone that is responsible for the stabilization and maturation of many oncogenic proteins. Therefore, Hsp90 has emerged as an attractive target in the field of cancer chemotherapy. In this study, we report the design, synthesis, and biological evaluation of a series of Hsp90 inhibitors. In particular, compound **30f** shows a significant Hsp90α inhibitory activity with IC_{50} value of 5.3 nM and an excellent growth inhibition with GI_{50} value of 0.42 μM against non-small cell lung cancer cells, H1975. Compound **30f** effectively reduces the expression levels of Hsp90 client proteins including Her2, EGFR, Met, Akt, and c-Raf. Consequently, compound **30f** promotes substantial cleavages of PARP, Caspase 3, and Caspase 8, indicating that **30f** induces cancer cell death via apoptotic pathway. Moreover, cytochrome P450 assay indicates that compound **30f** has weak inhibitory effect on the activities of five major P450 isoforms (IC_{50} > 5 μM for 1A2, 2C9, 2C19, 2D6, and 3A), suggesting that clinical interactions between **30f** and the substrate drugs of the five major P450 isoforms are not expected. Compound **30f** also inhibits the tumor growth in a mouse xenograft model bearing subcutaneous H1975 without noticeable abnormal behavior and body weight changes. The immunostaining and western immunoblot analysis of EGFR, Met, Akt in xenograft tissue sections of tumor further demonstrate a good agreement with the *in vitro* results.

1. Introduction

The molecular chaperone heat shock protein 90 (Hsp90) maintains protein homeostasis under numerous stressors by regulating the correct folding, stability, and activity of various client proteins [1–4]. Hsp90 clients include many oncogenic proteins, such as epidermal growth factor receptor (EGFR), human epidermal growth factor receptor 2 (Her2), mesenchymal-epithelial transition tyrosine receptor (Met), anaplastic lymphoma kinase (Alk), protein kinase B (Akt/PKB), cellular rapidly accelerated fibrosarcoma (c-Raf), cyclin-dependent kinase 4 (Cdk4), hypoxia-inducible factor 1α (Hif-1α), matrix metalloproteinase 2 (MMP2), mutant P53 and wee1, which are necessary for the development and progression of cancer. Due to the hostile environment in cancers such as hypoxia, acidosis, and nutrition deprivation, Hsp90 is overexpressed in cancer cells 2–10 fold higher than normal cells and exists as activated multi-chaperone complexes in cancer cells [5]. In this regard, cancer cells are highly addicted to Hsp90 chaperone function for the survival and proliferation. More importantly, inhibition of Hsp90 results in simultaneous blockage of multiple signaling pathways in cancers, overcoming the inevitable drug resistance of conventional chemotherapies. Therefore, inhibition of the molecular chaperone Hsp90 represents a promising chemotherapeutic strategy toward the treatment of various types of cancers.

Over the past decades, a substantial number of Hsp90 inhibitors have been developed [6–13]. The ansamycin antibiotic, geldanamycin (**1**) was first identified as an Hsp90 inhibitor in 1994 (Fig. 1) [14]. Since then, a number of geldanamycin analogues such as

* Corresponding author.
** Corresponding author.
E-mail addresses: hanne.md@gmail.com (E. Ha), seoyho@kmu.ac.kr (Y.H. Seo).
[1] Sun You Park and Yong Jin Oh contributed equally to this work.

https://doi.org/10.1016/j.ejmech.2017.11.054
0223-5234/

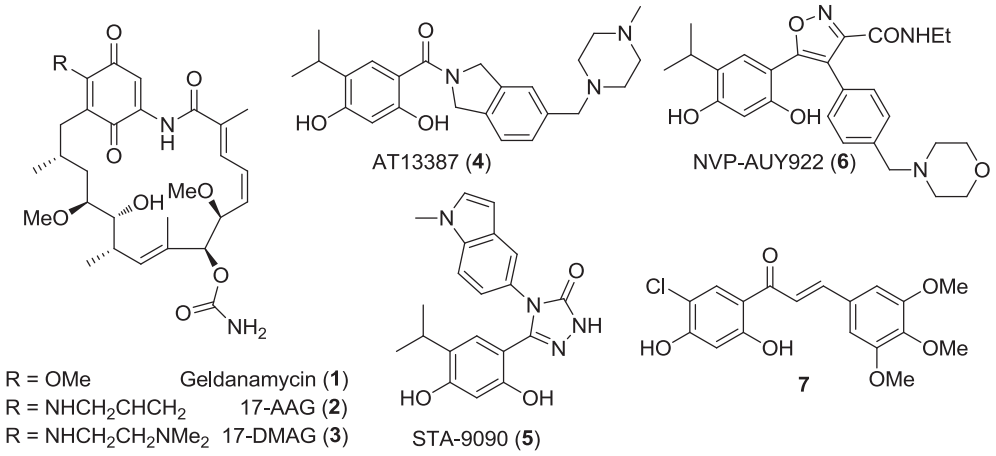

Fig. 1. Structure of Hsp90 inhibitors.

tanespimycin (17-AAG, **2**) and alvespimycin (17-DMAG, **3**) have been developed and entered into clinical studies [8]. However, the first-generation ansamycin derivatives engendered several drawbacks in the clinical applications including poor solubility and toxicity [15]. Consequently, substantial efforts had been directed towards finding different chemical scaffolds to improve pharmacological properties as well as safety profiles, resulting in the second-generation Hsp90 inhibitors. These second-generation Hsp90 inhibitors are classified into three major cores, purine, resorcinol, and benzamide. The purine class of Hsp90 inhibitors that mimics the adenine ring of natural nucleotide ligand ATP, includes PU-H71 [16], BIIB021 [17], and CUDC-305 [18] and resorcinol-based Hsp90 inhibitors include AT13387 (**4**) [19], STA-9090 (**5**) [20], NVP-AUY922 (**6**) [21]. The benzamide scaffold is another important class of Hsp90 inhibitors, which includes TAS-116 [22], XL888 [23] and SNX-5422 [24]. A number of the second-generation Hsp90 inhibitors have entered to the clinical trials and demonstrate an improved potency with lesser toxicities [6,25,26]. However, none of the Hsp90 inhibitors are clinically approved yet. Most recently, Hsp90 inhibitor STA-9090 has failed to demonstrate the clinical benefit in the phase III clinical trial due to the moderate efficacy and consequently the clinical trial has been terminated [26]. Although the clear reasons for the failure are still under investigation, acquired resistance to STA-9090 has been proposed as one possible reason [27]. In this regard, the discovery of Hsp90 inhibitors with different chemotypes is still a demanding task in this area.

As part of our ongoing effort to develop potent Hsp90 inhibitors, we have previously discovered a chalcone-based Hsp90 inhibitor (**7**) by utilizing a fragment-linking strategy [28–31]. Despite its potential as an anticancer drug, there are several challenges for its clinical application. One is that, owing to the intrinsic electrophilic characteristic of the enone moiety that acts as Michael acceptor, chalcone structure of compound **7** might exert a non-specific binding issue and render compound **7** susceptible to be attacked by endogenous cellular nucleophiles such as cysteine, lysine, and histidine [32,33]. Besides, there still remains a need for the improvement of the potency. Therefore, we decided to replace the enone moiety with various amide groups, ruling out the possibility of its non-specific binding events.

2. Results and discussion

2.1. Chemistry

Our synthesis began with preparation of benzyl amines **9a-h**. Reductive amination of benzaldehydes **8a-h** with methyl amine and sodium borohydride gave benzyl amines **9a-h** in 22–100% yields (Scheme 1). Alternatively, benzoic acids **10a-b** was converted to amides **11a-b** in 11–41% yields using EDC, HOBt and DIPEA in DMF, which was then reduced using lithium aluminum hydride to furnish benzyl amines **12a-b** in 65–81% yields.

We next synthesized compound **20** and **21a-h**, which had chloro substituent on resorcinol ring (Scheme 2). The synthesis of **20** and **21a-h** commenced with esterification of commercially available **13**, providing ester **14** in 86% yield. Subsequent chlorination of **14** with sulfuryl chloride in dichloromethane gave **15** in 45% yield. Compound **15** was then protected with allyl bromide and potassium carbonate in DMF, quantitatively to furnish compound **16**. Compound **16** was hydrolyzed with sodium hydroxide in methanol and water to give carboxylic acid **17** in 80% yield. With carboxylic acid **17** and amine **9a-h** in hand, we carried out amide coupling reactions of **17** with **9a-h** or benzyl amine using EDC, HOBt and DIPEA in DMF, followed by cleavage of allyl-protecting group using $PdCl_2(PPh_3)_2$ reaction, consequently to provide compound **20** and **21a-h** in 21–90% yields in two steps. Although the synthetic route in Scheme 2 successfully provided compound **20** and **21a-h**, it required a lengthy synthesis with an additional protection and deprotection reaction steps. Besides, the yield of allyl cleavage reaction was unexpectedly low. Hence, we examined the viability of direct amide coupling reaction of **22** without protecting group. To do so, we first hydrolyzed the ester **15** with sodium hydroxide in methanol and water to obtain carboxylic acid **22** in quantitative yield. With **22** in hand, we carried out amide coupling reaction of **22** with amine **12a-b**. To our delight, the reaction using EDC, HOBt and DIPEA in DMF at 120 °C under microwave irradiation afforded compound **23a-b** in 69% and 26% yield.

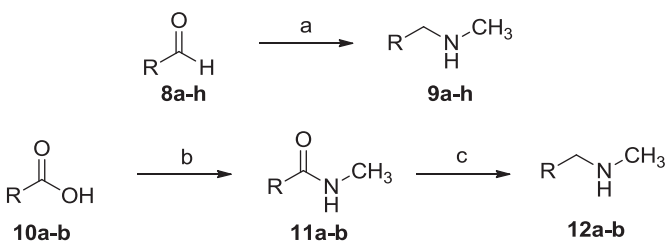

Scheme 1. Synthesis of compound **9a-h** and **12a-b**[a]
[a]Reagents and conditions: (a) CH_3NH_2, $NaBH_4$, MeOH, 0 °C, 1.5 h; (b) CH_3NH_2, EDC, HOBt, DIPEA, DMF, microwave, 120 °C, 30 bar, 3 h; (c) $LiAlH_4$, THF, 0 °C, 12 h.

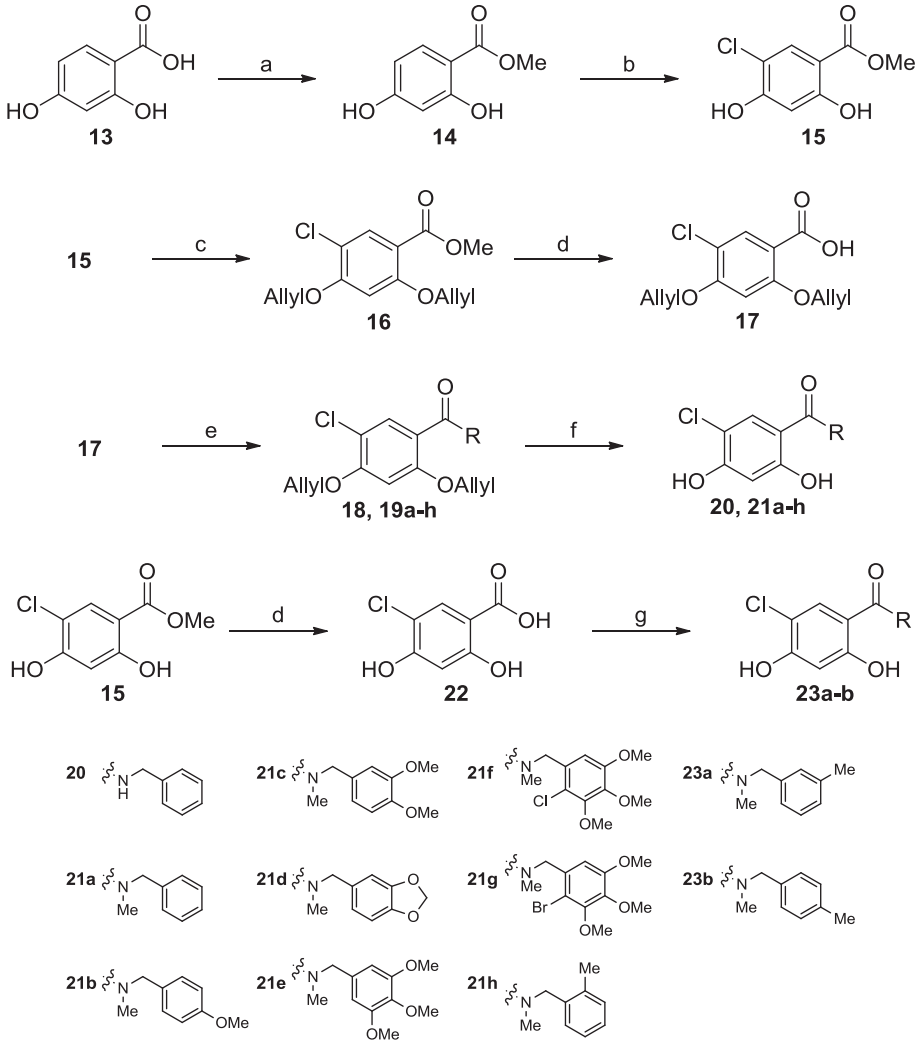

Scheme 2. Synthesis of compound **20** and **21a-h**[a]
[a]Reagents and conditions: (a) H_2SO_4, MeOH, 100 °C, 24 h; (b) SO_2Cl_2, DCM, 0 °C, 24 h; (c) Allyl bromide, K_2CO_3, DMF, rt, 24 h; (d) NaOH, MeOH-H_2O, rt, 30 h; (e) amines for **18** and **19a-h**, DCC, HOBt, DIPEA, DMF, μW, 120 °C, 30 bar, 3 h; (f) $PdCl_2(PPh_3)_2$, NH_4HCO_2, THF, microwave, 120 °C, 30 bar, 1 h; (g) amines, EDC, HOBt, DIPEA, DMF, microwave, 120 °C, 30 bar, 3 h.

2.2. *In vitro assays of compounds **20**, **21a-h** and **23a-b***

Upon completion of synthesis, compound **20**, **21a-h** and **23a-b** were evaluated for the binding affinity to human recombinant Hsp90α and the anti-proliferative activity against Skbr3 and H1975 cell lines. Skbr3 is a human breast cancer cell line that overexpresses Her2, and H1975 is a gefitinib-resistant non-small cell lung cancer (NSCLC) cell line. Encouragingly, as shown in Table 1, most of compounds exhibited appreciable Hsp90 inhibition activity and good cellular efficacy against Skbr3 and H1975. Notably, Skbr3 responded more sensitively than H1975 to the exposure of compound **21a-h** and **23a-b**. Since Her2 is well-known Hsp90-dependent substrate, we assumed that Her2 overexpressing Skbr3 was more susceptible to inhibition of Hsp90 than H1975. Interestingly, compound **20** derived from primary amine was much less potent than tertiary amide **21a**, probably because intramolecular hydrogen bonding of secondary amide NH with adjacent 2′-hydroxy group did not allow the favorable binding conformation in the ATP-binding pocket of Hsp90 [34]. *Para*-methoxy-substituted analogue **21b** afforded the strongest binding affinity to Hsp90α as well as the most potent anti-proliferative effect on Skbr3 and H1975. In contrast, *meta*-substituents on phenyl ring exerted a negative impact on the binding affinity to Hsp90α and the anti-proliferative effect on Skbr3 and H1975. For example, *meta*-substituted analogues **21c-e** displayed the lower binding affinity to Hsp90α and less potency against Skbr3 and H1975 than **21b**. IC_{50} value of 3,4,5-trimethoxy substituted analogue **21e** to Hsp90α was larger than 1 μM, indicating that there were spatial or electrical repulsions and alterations of optimal interactions to ATP-binding pocket. It is noteworthy that introducing bromo or chloro group at *ortho*-position of **21e** significantly increased the binding affinity to Hsp90α and the anti-proliferative activity against Skbr3 and H1975. Consistently, the introduction of methyl substituent at *para*-position of the phenyl ring (**23b**) did not have deleterious effect on Hsp90 inhibition and cancer cell growth inhibition, while the introduction of methyl substituent at *meta*-position (**23a**) was deleterious toward Hsp90 inhibition and cancer cell growth inhibition.

2.3. *Synthesis of compounds **30a-f***

To optimize the binding affinity of ligands to Hsp90α, we set out

Table 1
Binding affinity to Hsp90α and anti-proliferative activity of compound **20**, **21a-h**, and **23a-b**.

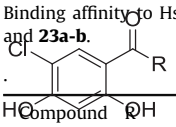

Compound	R	Hsp90α (FP)[a] (IC_{50}; nM)	Skbr3[b] (GI_{50}; μM)	H1975[b] (GI_{50}; μM)
GA		14.0 ± 1.4	NA	0.56 ± 0.02
20	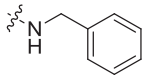	>1000	NA	86.2 ± 2.3
21a	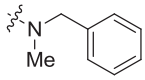	413 ± 33.2	18.3 ± 1.6	35.5 ± 2.3
21b	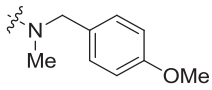	135 ± 21.2	7.2 ± 0.7	16.7 ± 1.3
21c	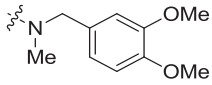	362 ± 40.0	7.7 ± 1.2	33.4 ± 1.3
21d	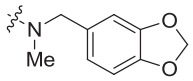	585 ± 15.2	41.8 ± 2.6	103 ± 2.5
21e	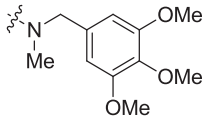	>1000	30.1 ± 1.9	73.1 ± 0.5
21f	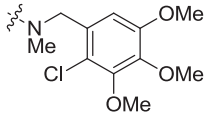	429 ± 11.0	2.4 ± 0.4	33.8 ± 2.2
21g	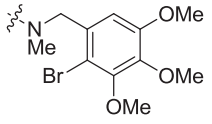	528 ± 36.0	7.7 ± 0.2	34.3 ± 1.2
21h	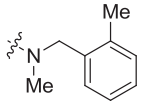	995 ± 46.0	4.2 ± 1.3	47.5 ± 2.6
23a	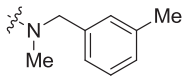	830 ± 30.6	11.3 ± 2.9	49.3 ± 0.1
23b	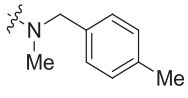	558 ± 4.9	7.2 ± 0.1	34.3 ± 1.9

[a] Binding to N-terminal domain of Hsp90α was determined by a fluorescence polarization (FP) assay.
[b] GI_{50} values were obtained after the treatment of cells for 72 h.

to apply fragment-growing strategy, guided by docking pose of **21a** on Hsp90α (Fig. 2). We first performed docking simulations of **21a** with Hsp90α (PDB code: 2XJX) as a template protein. The docking study indicated that the resorcinol ring of **21a** formed two hydrogen bonding interactions with the carboxylate side chain of Asp93 and conserved water in the deep cavity of ATP-binding pocket. The carbonyl group of **21a** formed a hydrogen bonding interaction with the hydroxyl group of Thr184. Interestingly, the pendant phenyl group of **21a** was located in close proximity to Asp102 and Asn106 and there was spatial cleft toward *para*-position of phenyl ring, explaining substituent effect observed in a

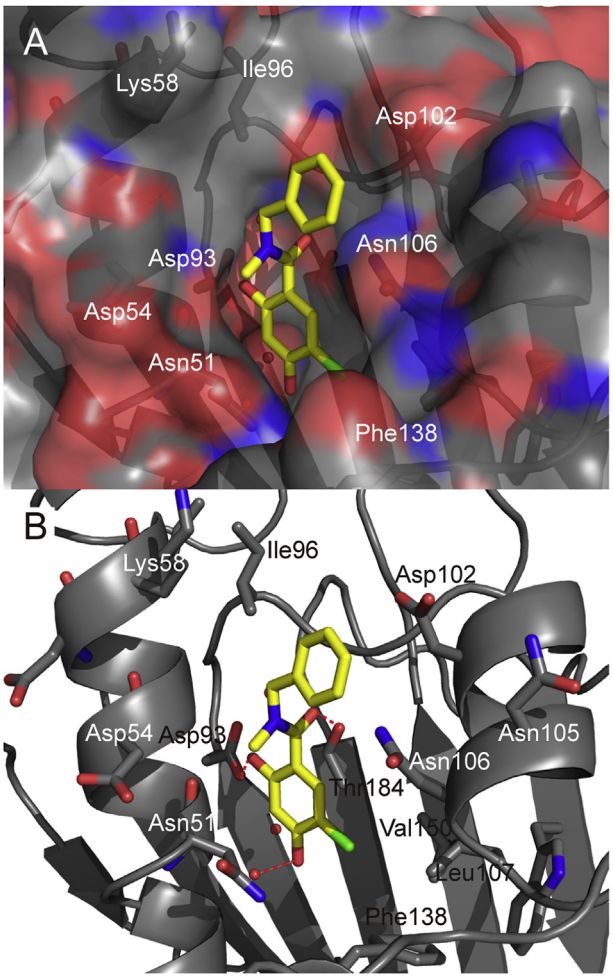

Fig. 2. (A) Molecular docking model of **21a** in the ATP-binding pocket of human Hsp90α (PDB code: 2XJX) shown in surface representation. (B) Cartoon and sticks representation of Hsp90α and **21a** complex. The carbon, oxygen, nitrogen, and chloro atoms of **21a** are shown in yellow, red, blue, and green. The side chains of the binding site are colored by atom types (carbon, gray; oxygen, red; nitrogen, blue) and labeled with their residue name. Water molecules are shown as red spheres and hydrogen bonds in dashed red lines. The docking poses were visualized using PyMOL1.3. (For interpretation of the references to colour in this figure legend, the reader is referred to the web version of this article.)

series of compounds in Table 1. Based on 3D structure of Hsp90-**21a** complex, we assumed that the *para*-position of the phenyl ring could be the best place for fragment-growing, possibly having a positive impact on its binding affinity to Hsp90α. Besides, the binding affinity of a series of compounds shown in Table 1 supported the assumption as well. Therefore, we decided to modify the *para*-position of the phenyl ring in compound **21a** with amide moiety, anticipating that amide substituent could form additional hydrogen bonds with the neighboring carboxylate side chain of Asp102 and amide side chain of Asn106.

To test the hypothesis, we synthesized compound **30a-f** (Schemes 3 and 4). Isopropyl group is a common moiety found in resorcinol-based Hsp90 inhibitors and it has been reported that the replacement of chloro group with isopropyl improves the potency of compound by forming proximal lipophilic interactions with the hydrophobic amino acid residues in ATP-binding pocket [19]. Thus, we pursued the synthesis of isopropyl analogues along with chloro analogues. Firstly, compound **25** was synthesized following the previously reported procedure [35]. Briefly, Friedel-Crafts alkylation of compound **14** with isopropyl bromide in the presence of

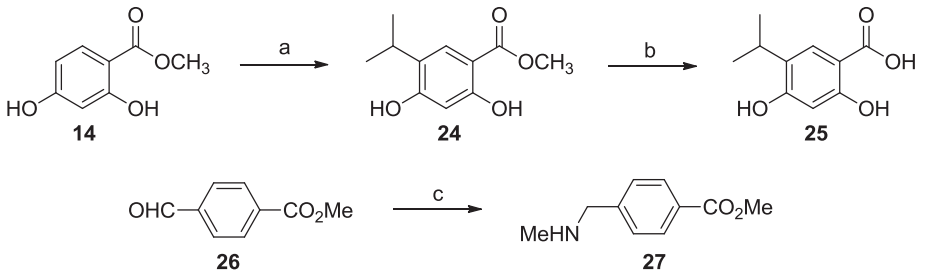

Scheme 3. Synthesis of compound **25** and **27**[a]
[a]Reagents and conditions: (a) *i*-PrBr, $AlCl_3$, DCM, 60 °C, 18 h; (b) LiOH, MeOH-H_2O (1: 1), rt, 30 h; (c) CH_3NH_2, $NaBH_4$, MeOH, 0 °C, 1.5 h.

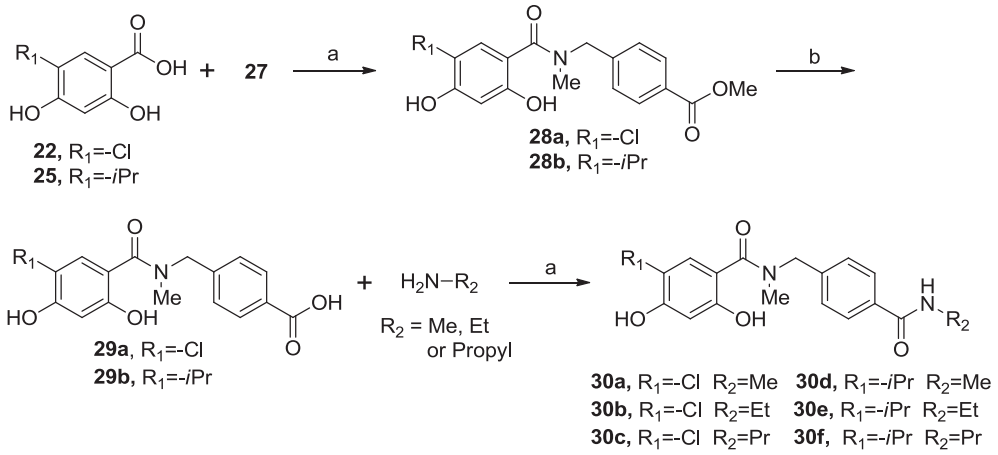

Scheme 4. Synthesis of compound **30a-f**[a]
[a]Reagents and conditions: (a) EDC, HOBt, DIPEA, DMF, μW, 120 °C, 30 bar, 3 h; (b) NaOH, MeOH-H_2O (1: 1), rt, 30 h.

aluminum chloride provided **24** in 46% yield. Subsequent hydrolysis of **24** with lithium hydroxide gave carboxylic acid **25** in 100% yield. With carboxylic acid **25** in hand, we next synthesized amine **27**. Reductive amination of **26** with methyl amine and sodium borohydride gave amine **27** in 81% yield.

Having prepared compound **22**, **25**, and **27**, we then performed amide coupling reaction of **22** or **25** with **27**using EDC, HOBt, and DIPEA in DMF, which afforded compound **28a-b** in 76–82% yields (Scheme 4). The resulting **28a-b** were subsequently subjected to hydrolysis in the presence of lithium hydroxide to give carboxylic acid **29a-b** in 85–88% yield. Finally, amide coupling reaction of **29a-b** with primary alkyl amine (R_2 = methyl, ethyl, or propyl) smoothly provided the desired product **30a-f** in 17–46% yields.

2.4. Comparative in vitro assays of compounds *30a-f*

With compound **30a-f** in hand, we examined the impact of *N*-alkyl amide attached to phenyl ring of chloro and isopropyl analogues. H1975 is a gefitinib-resistant cell line, acquired by EGFR mutation and Met amplification. Given that both EGFR and Met are clients of Hsp90, H1975 cell line may be best suited to evaluate Hsp90 inhibitors. Therefore, the prepared compound **30a-f** were tested for the anti-proliferative activity against H1975 cell line as well as the binding affinity to Hsp90α. In general, chloro analogue **30a-c** led to lower binding affinity to Hsp90α and lower cellular efficacy against H1975 than isopropyl analogue **30d-f**, as expected. Surprisingly, compound **30f**, having *N*-propyl amide and isopropyl moiety displayed a significant enhancement of Hsp90 binding affinity (IC_{50} = 5.3 nM) and cellular efficacy (GI_{50} = 0.42 μM) against H1975. To determine binding kinetics of compound **30f** with Hsp90α, we also performed surface plasmon resonance (SPR) assay and the data clearly indicated that compound **30f** strongly bound to Hsp90α with K_D value of 3.08 nM (Supplementary Fig. 1). At this point in the discovery effort, **30f** represented the most advanced analogue. It demonstrated the strongest binding affinity to Hsp90α and the most potent cellular activity .

Hsp90α potency (pIC_{50}) of all synthesized compounds was plotted against lipophilicity (clogP), in that diagonal lines represent contours of equal lipophilic efficiencies (LipE = pIC_{50} − clogP), which is an important parameter to evaluate the quality of small molecules, linking potency and lipophilicity (Fig. 3) [36,37]. Analogues **20**, **21a-h**, and **23a-b** in Table 1 and chloro analogues **30a-c** in Table 2 provided relatively low LipE values, all of which were less than 5 LipE values. Interestingly, all isopropyl analogues **30d-f** possessed LipE values greater than 5, indicating that installing isopropyl group significantly enhanced Hsp90α potency, pIC_{50} without appreciable increase in lipophilicity, clogP.

2.5. Molecular docking modeling of compound *30f*

Modeling compound **30f** into the ATP-binding pocket of human Hsp90α (PDB code: 2XJX) indicated that **30f** occupied a deep ATP-binding pocket in the N-terminal domain of Hsp90α, where the resorcinol ring of **30f** formed an extensive network of hydrogen bonds with the carboxylate side chain of Asp93 and highly ordered water molecules trapped in the bottom of the pocket (Fig. 4). The modeling also indicated that carbonyl group of **30f** interacted with the hydroxyl side chain of Thr184 and a conserved water, to form two hydrogen bonds. Furthermore, the isopropyl moiety of **30f** formed hydrophobic interactions with lipophilic side chains of

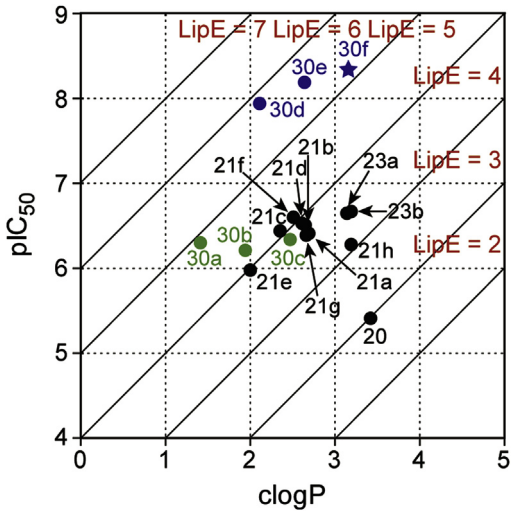

Fig. 3. clogP *vs* pIC_{50} plot and LipE analysis. Analogues **20**, **21a-h**, and **23a-b** in Table 1 are plotted in black. Chloro analogues **30a-c** and isopropyl analogues **30d-f** in Table 2 are plotted in green and blue, respectively. (For interpretation of the references to colour in this figure legend, the reader is referred to the web version of this article.)

Table 2
Binding affinities to Hsp90α and anti-proliferative activities of compound **30a-f**.

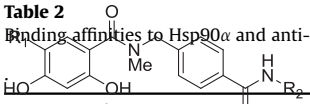

Compound	R_1	R_2	Hsp90α (FP)[a] (IC_{50}; nM)	H1975[b] (GI_{50}; μM)
GA			14.0 ± 1.4	0.56 ± 0.02
21a			413.0 ± 33.2	35.5 ± 2.3
30a			496.0 ± 133	34.8 ± 0.8
30b			611.5 ± 119	21.7 ± 2.9
30c			454.0 ± 63.5	20.8 ± 4.0
30d			11.4 ± 7.0	0.86 ± 0.07
30e			6.5 ± 0.3	0.46 ± 0.07
30f			5.3 ± 2.4	0.42 ± 0.01

[a] Binding to N-terminal domain of Hsp90α was determined by a fluorescence polarization (FP) assay.
[b] GI_{50} values were obtained after the treatment of cells for 72 h.

Leu107, Val150, and Phe138. The hydrophobic interactions of the isopropyl moiety of compound **30d-f** proved to be critical, in that the binding affinity of **30d-f** to Hsp90α was approximately 40–100 folds higher than that of **30a-c** (Table 2). The binding pose of **30f** represented that *N*-propyl amide substituent on phenyl ring formed additional two hydrogen-bonding interactions with the carboxylate of Asp102 and the amide of Asn106 residues, as we anticipated by fragment-growing drug design from compound **21a** in Fig. 2.

2.6. Biological evaluation of compound *30f*

To assess the dose and time dependent effect of **30f** on the growth of cancer cells, we treated H1975 cells with **30f** at various concentrations for 0, 1, 2, and 3 days. Compound **30f** potently blocked the growth of H1975 cells in a dose and time dependent

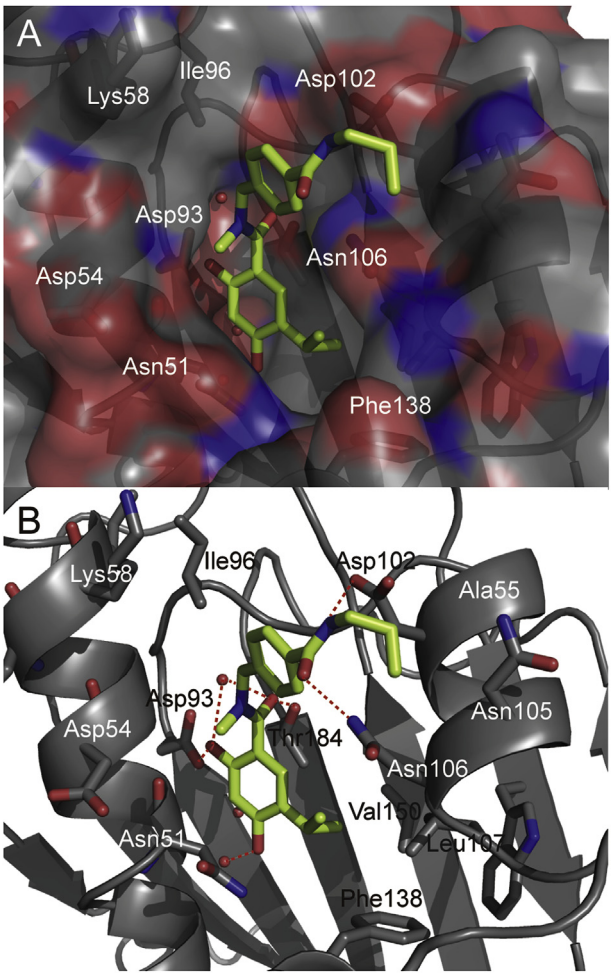

Fig. 4. (A) Molecular docking model of **30f** bound in the ATP-binding pocket of human Hsp90α (PDB code: 2XJX) shown in surface representation. (B) Cartoon and sticks representation of Hsp90α and **30f** complex. The carbon, oxygen and nitrogen atoms of **30f** are shown in green, red, and blue. The side chains of binding site are colored by atom types (carbon, gray; oxygen, red; nitrogen, blue) and labeled with their residue name. Water molecules are shown as red spheres and hydrogen bonds are shown in dashed red lines. The docking poses were visualized using PyMOL1.3. (For interpretation of the references to colour in this figure legend, the reader is referred to the web version of this article.)

manner. To further examine the effect of **30f** on Hsp90 dependent signaling pathways, we measured the expression levels of Hsp90 client proteins in H1975 cells. It is well documented that a cellular biomarker of Hsp90 inhibition is the degradation of client proteins, with concomitant induction of Hsp70. As shown in Fig. 5B, the treatment of H1975 with **30f** significantly reduced expression of EGFR, Her2, Met, Akt, and c-Raf, while **30f** increased protein levels of Hsp70 and Hsp90. The expression level of internal standard, β-actin remained unchanged. The concentration of **30f**, which was needed to furnish anti-proliferative activity, paralleled the concentration needed to promote the degradation of Hsp90 clients, clearly indicating that the anti-proliferative effect of **30f** on cancer cells was a consequence of Hsp90 inhibition.

Upon treatment of H1975 with **30f**, substantial cleavages of PARP, Caspase 3, and Caspase 8 were observed. The result indicated that **30f** promoted apoptotic cell death of H1975 cells. Interestingly, compound **30f** did not alter the expression level of Bcl-2 and Bax, suggesting that **30f** activated the apoptosis of H1975 cells through the extrinsic apoptotic pathway.

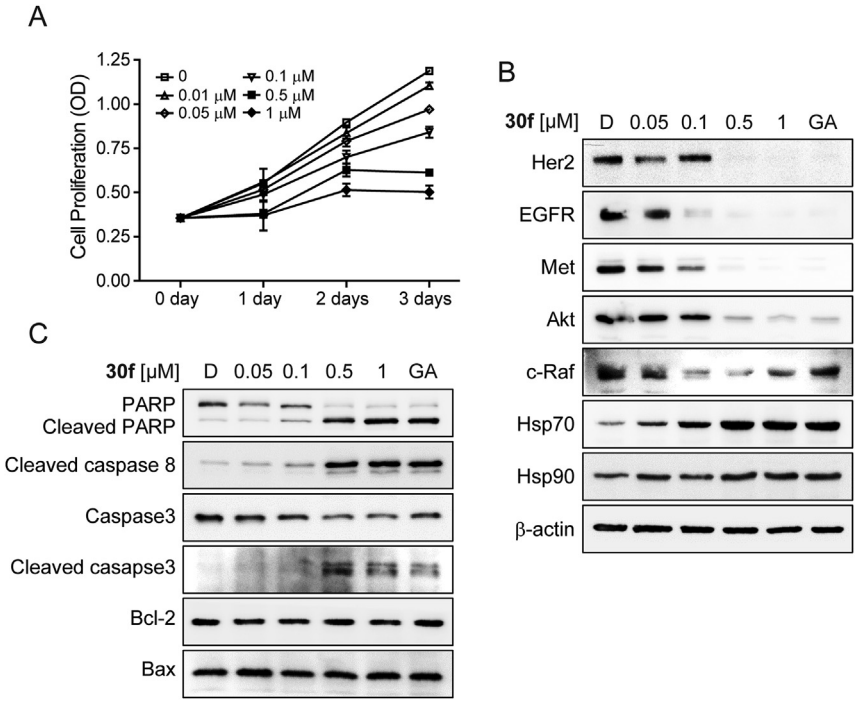

Fig. 5. (A) Effect of **30f** on the proliferation of H1975. Cells were incubated with indicated concentrations of **30f** for 0, 1, 2, and 3 days and cell proliferation was measured by MTS colorimetric assay. (B) Effect of **30f** on expression of Her2, EGFR, Met, c-Raf, Akt, Hsp70 and Hsp90. (C) Effect of **30f** on apoptotic biomarkers. H1975 cells were incubated with the indicated concentrations of **30f** for 24 h and the expression of Hsp90 clients and apoptotic biomarker proteins were analyzed by western blot. Geldanamycin (GA, 1 μM) and DMSO (D) were used as a positive and a negative control, respectively.

2.7. *Effect of compound **30f** on cytochrome P450s*

Cytochrome P450 (P450) enzymes have emerged as an important determinant in the occurrence of drug interactions that can lead to adverse drug reactions. Therefore, we investigated the effect of compound **30f** on the catalytic activities of clinically significant human P450s such as 1A2, 2C9, 2C19, 2D6, and 3A in human liver microsomes [38,39]. To do so, the inhibitory potency of compound **30f** was determined with cytochrome P450 assays in the absence and the presence of compound **30f** up to 50 μM final concentration using pooled human liver microsomes (Table 3). The assay indicated that compound **30f** showed weak inhibitory effect (> 5 μM) against five P450 isoforms. These findings suggest that clinical interactions between compound **30f** and substrate drugs of five P450 isoforms would not be expected.

2.8. *In vivo anticancer effect of compound **30f***

To determine whether *in vitro* effects of **30f** translate into *in vivo* model, we subcutaneously injected NOD-scid IL2Rgammanull mice (NSG) mice with H1975 human non-small lung cancer cells (2.0×10^6 cells/mice). One weeks after xenotransplantation of H1975 cells, we administered compound **30f** intraperitoneally (25 and 50 mg/kg) during weekdays followed by weekend rest for 3 weeks. We determined body weight from the first injection day of compound **30f** (day 0) to the end of experimental period (day 21) and found no difference in body weight, treatment-related deaths, and abnormal behaviors among vehicle and experimental groups (Fig. 6B), which implicated that compound **30f** was well tolerated at the dose levels of both 25 and 50 mg/kg. Mice injected with vehicle control developed visible tumors that grew continuously throughout the course of the treatment period. In contrast, mice injected with 25 and 50 mg/kg compound **30f** exhibited delayed tumor growth starting approximately 10 days after the treatment. The growth rates of the tumors were delayed at 16 days after the treatment and were continuously delayed to the end of experimental period (Fig. 6A). Consistent with *in vitro* results, compound **30f** treatment *in vivo* resulted in decreased expressions of EGFR, Met, and Akt evidenced by immunoblot (Fig. 6C) and immunohistochemistry (Fig. 6D) assays.

Table 3
Inhibitory potency of compound **30f** on specific P450 activities in human liver microsomes.

Enzyme activity	P450	IC_{50} (μM)
Phenacetin *O*-deethylation	1A2	34.1
Tolbutamide 4-methylhydroxylation	2C9	5.3
Omepraozle hydroxylation	2C19	14.6
Dextromethorphan *O*-demethylation	2D6	23.0
Midazolam 1′-hydroxylation	3A	25.9

3. Conclusion

In the current study, the design, synthesis, and biological evaluation of a series of Hsp90 inhibitors have been described. With the aid of computational docking simulation followed by fragment-growing strategy, we were able to systematically design and optimize Hsp90 inhibitor, **30f**. Moreover, compound **30f**, which was structurally simple and easily synthesized in 5 steps from commercially available methyl 2,4-dihydroxybenzoate, demonstrated an exceptionally potent binding affinity to the N-terminus of Hsp90α ($IC_{50} = 5.3$ nM) in the FP assay, approximately one-third lower than a well-known Hsp90 inhibitor, geldanamycin (GA, $IC_{50} = 14.0$ nM). Compound **30f** showed inhibitory effect on the proliferation of H1975 NSCLC cells with GI_{50} value of 0.42 μM, which was significantly less GI_{50} concentration than the ones we previously reported [31]. The expression levels of oncogenic proteins, Her2, EGFR, Met, Akt, and c-Raf, in H1975 cells treated with compound **30f** dose-dependently decreased while that of Hsp70

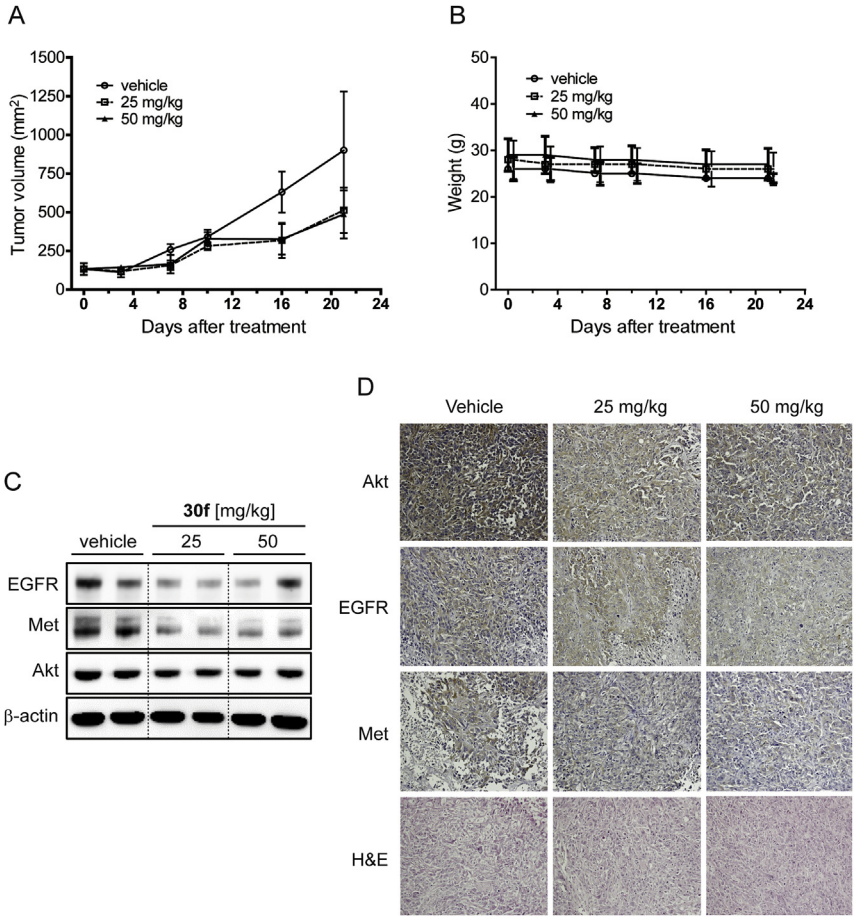

Fig. 6. (A) Antitumor activity of compound **30f** in a mouse xenograft model. (A) The average volumes of the H1975-derived tumors from the vehicle and **30f** treated mice were plotted 3 weeks after tumor inoculations. (B) Body weight changes were recorded during the treatment of vehicle and **30f**. (C) Immunoblot analyses of EFGR, Met, and Akt in H1975 xenograft tissues. (D) Immunostaining of Akt, EGFR, Met, and H&E in H1975 xenograft tissue sections.

increased, indicating the characteristic molecular biomarkers of Hsp90 inhibition. Western immunoblot analysis also revealed that **30f** induced PARP, Caspase 3 and Caspase 8 cleavages, suggesting that compound **30f** promoted apoptotic cell death of H1975 cells. Cytochrome P450 assay indicated that **30f** exhibited weak inhibitory effect against five P450 isoforms (IC_{50} > 5.0 μM for 1A2, 2C9, 2C19, 2D6, and 3A), suggesting that interactions between compound **30f** and substrate drugs of the five P450 isoforms under physiological environment are not expected. Moreover, compound **30f** displayed a significant *in vivo* inhibitory effect on tumor growth and in a mouse xenograft model bearing subcutaneous H1975 tumors. Importantly, no noticeable abnormal behavior and body weight changes were observed in mice treated with compound **30f**. The immunostaining and western immunoblot analyses of Akt, EGFR, and Met in xenograft tissue sections of tumor also demonstrated a good agreement with the *in vitro* results.

Overall, the attractive attributes of compound **30f** warranted further studies on ADMET profile and its therapeutic evaluation for various types of cancer. These studies will be reported in due course.

4. Experimental

4.1. Chemistry

4.1.1. General methods and materials

All reagents and solvents were purchased from Sigma-Aldrich (Milwaukee Wisconsin, USA), and Alfa Aesar (Massachusetts, USA), and used without further purification. All experiments dealing with moisture-sensitive compounds were carried out under argon atmosphere. Concentration or solvent removal under reduced pressure was carried out using rotary evaporator. Analytical thin layer chroatography was performed on precoated silica gel F_{254} TLC plates (E, Merck) with visualization under UV light. Column chromatography was conducted under medium pressure on silica (Merck Silica Gel 40–63 μm) or performed by using a Biotage SP1 flash purification system with prepacked silica gel cartrides (Biotage). NMR analyses were carride out using a JNM-ECZ500R (500 MHz) manufactured by Jeol resonance. Chemical shifts are reported in parts per million (δ). The deuterium lock signal of the sample solvent was used as a reference, and coupling constants (J) are given in hertz (Hz). The splitting pattern abbreviations are as follows: s, singlet; d, doublet; t, triplet; q, quartet; dd, doublet of doublets; m, multiplet. The purities of all final compounds were confirmed to be higher than 95% by analytical HPLC performed with a dual pump Shimadzu LC-6AD system equipped with VP-ODS C18 column (4.6 mm × 250 mm, 5 μm, Shimadzu).

4.1.2. (2-Chloro-3,4,5-trimethoxyph4enyl)-N-methylmethanamine (**9f**)

5-Chloro-2,3,4-trimethoxybenzaldehyde (1.01 g, 4.35 mmol) and 40% methylamine (0.20 g, 6.54 mmol) in methanol was stirred at room temperature for 30 min. Sodium borohydride (0.08 g, 2.18 mmol) was added at 0 °C and was stirred for 1 h. The mixture

was added water, methanol removed under reduced pressure and then extracted with dichloromethane three times. The organic layer was dried over Na_2SO_4, concentrated under reduced pressure to afford compound **9f** in 89% yield. ^{1}H NMR (500 MHz, CD_3OD) δ 6.88 (s, 1H), 4.89 (s, 1H), 3.85 (s, 3H), 3.84 (s, 3H), 3.82 (s, 3H), 3.77 (s, 2H), 2.39 (s, 3H). ^{13}C NMR (125 MHz, CD_3OD) δ 153.6, 151.1, 143.7, 133.4, 120.4, 110.2, 61.5, 61.4, 56.6, 53.4, 35.4.

*4.1.3. General procedure for the synthesis of compounds (**20** and **21a-h**)*

Compound **17** (1 equiv) was added to a benzyl amine or benzyl amine derivatives (**19a-h**) (1.5 equiv), *N*,*N*-dicyclohexylcarbodiimide (2 equiv), 1-hydroxybenzotriazole monohydrate (1 equiv) and *N*,*N*-diisopropylethylamine (1 equiv) in DMF. The reaction mixture was stirred under microwave irradiation at 120 °C for 3 h. After completion of the reaction, the mixture was dissolved in ethyl acetate. The organic layer was washed with saturated 1N-HCl three times, dried over Na_2SO_4, concentrated under reduced pressure and purified by MPLC or column chromatography to afford intermediate compound. The resulting intermediate compound was stirred under microwave irradiation for 1 h at 120 °C in the presence of $PdCl_2(PPh_3)_2$ (0.05 equiv) and ammonium formate (2.5 equiv) in THF. The reaction mixture was diluted with ethyl acetate. The organic layer was washed with water, dried over Na_2SO_4, concentrated under reduced pressure and purified by MPLC to afford compound **20** and **21a-h** in 21–90% yield.

*4.1.3.1. N-Benzyl-5-chloro-2,4-dihydroxybenzamide (**20**).* 53% yield. R_f = 0.37 (3:7 ethyl acetate: hexane). ^{1}H NMR (500 MHz, CD_3OD) δ 7.80 (s, 1H), 7.32–7.28 (m, 4H), 7.24–7.21 (m, 1H), 6.44 (s, 1H), 4.53 (s, 2H). ^{13}C NMR (125 MHz, CD_3OD) δ 170.0, 161.8, 158.9, 140.0, 130.0, 129.5, 128.4, 128.2, 112.9, 109.7, 105.0, 43.9. ESI MS (*m*/*e*) 278.05 $[M+1]^+$. Purity: 95.8% by HPLC.

*4.1.3.2. N-Benzyl-5-chloro-2,4-dihydroxy-N-methylbenzamide (**21a**).* 62% yield. R_f = 0.28 (2:3 ethyl acetate: hexane). ^{1}H NMR (500 MHz, CD_3OD) δ 7.32–7.22 (m, 4H), 7.12 (d, *J* = 6.5 Hz, 1H), 6.76 (d, *J* = 25.0 Hz, 1H), 6.47 (s, 1H), 5.88 (s, 1H), 4.55 (d, *J* = 52.0 Hz, 2H), 3.32 (s, 1H), 2.86 (d, *J* = 10.5 Hz, 3H). ^{13}C NMR (125 MHz, $CDCl_3$) δ 170.3, 155.1, 154.1, 136.7, 128.7, 128.3, 127.4, 127.2, 120.9, 115.9, 111.3, 107.8, 103.7, 101.0. ESI MS (*m*/*e*) 292.07 $[M+1]^+$. Purity: 100.0% by HPLC.

*4.1.3.3. 5-Chloro-2,4-dihydroxy-N-(4-methoxybenzyl)-N-methylbenzamide (**21b**).* 63% yield. R_f = 0.27 (2:3 ethyl acetate: hexane). ^{1}H NMR (500 MHz, $CDCl_3$) δ 7.29 (s, 1H), 7.21 (d, *J* = 8.5 Hz, 2H), 6.91 (dd, *J* = 6.5 Hz, 2.4 Hz, 2H), 6.64 (s, 1H), 4.65 (s, 2H), 3.82 (s, 3H), 3.05 (s, 3H). ^{13}C NMR (125 MHz, $CDCl_3$) δ 171.2, 160.6, 159.4, 155.0, 129.1, 128.7, 128.1, 114.4, 110.8, 110.1, 105.2, 55.5. 53.0, 36.8. ESI MS (*m*/*e*) 322.07 $[M+1]^+$. Purity: 99.7% by HPLC.

*4.1.3.4. 5-Chloro-N-(3,4-dimethoxybenzyl)-2,4-dihydroxy-N-methylbenzamide (**21c**).* 64% yield. R_f = 0.22 (1:1 ethyl acetate: hexane). ^{1}H NMR (500 MHz, CD_3OD) δ 7.16 (s, 1H), 6.91 (d, *J* = 8.5 Hz, 2H), 6.85 (s, 1H), 6.50 (s, 1H), 4.59 (s, 2H), 3.82 (s, 6H), 2.89 (s, 3H). ^{13}C NMR (125 MHz, CD_3OD) δ 170.2, 155.1, 153.8, 149.4, 148.5, 129.3, 128.7, 120.0, 116.0, 111.5, 111.2, 110.8, 103.3, 55.1, 55.0, 48.2, 29.4. ESI MS (*m*/*e*) 352.09 $[M+1]^+$. Purity: 96.2% by HPLC.

*4.1.3.5. N-(Benzo[d][1,3]dioxol-5-ylmethyl)-5-chloro-2,4-dihydroxy-N-methylbenzamide (**21d**).* 78% yield. R_f = 0.23 (2:3 ethyl acetate: hexane). ^{1}H NMR (500 MHz, $CDCl_3$) δ 7.29 (s, 1H), 6.81–6.73 (m, 3H), 6.63 (s, 1H), 5.97 (s, 2H), 4.61 (s, 2H), 3.05 (s, 3H). ^{13}C NMR (125 MHz, $CDCl_3$) δ 171.2, 160.4, 155.0, 148.3, 147.4, 129.9, 128.7, 121.2, 110.7, 110.2, 108.6, 108.2, 105.2, 101.3, 53.2, 36.8. ESI MS (*m*/*e*) 336.06 $[M+1]^+$. Purity: 99.0% by HPLC.

*4.1.3.6. 5-Chloro-2,4-dihydroxy-N-methyl-N-(3,4,5-trimethoxybenzyl)benzamide (**21e**).* 67% yield. R_f = 0.26 (3:2 ethyl acetate: hexane). ^{1}H NMR (500 MHz, $CDCl_3$) δ 7.27 (s, 1H), 6.61 (s, 1H), 6.49 (s, 2H), 4.62 (s, 2H), 3.84 (s, 9H), 3.06 (s, 3H). ^{13}C NMR (125 MHz, $CDCl_3$) δ 171.3, 159.6, 155.2, 153.7, 137.4, 131.9, 128.6, 111.2, 110.5, 105.2, 104.5, 61.0, 56.3, 53.7, 36.8. ESI MS (*m*/*e*) 382.10 $[M+1]^+$. Purity: 100.0% by HPLC.

*4.1.3.7. 5-Chloro-N-(2-chloro-3,4,5-trimethoxybenzyl)-2,4-dihydroxy-N-methylbenzamide (**21f**).* 42% yield. R_f = 0.20 (1:1 ethyl acetate: hexane). ^{1}H NMR (500 MHz, CD_3OD) δ 7.17 (s, 1H), 6.94 (s, 1H), 6.51 (s,1H), 4.74 (s, 2H), 3.86 (s, 3H), 3.85 (s, 3H), 3.83 (s, 3H), 2.99 (s, 3H). ^{13}C NMR (125 MHz, CD_3OD) δ 171.9, 156.9, 155.1, 154.1, 151.3, 143.6, 130.9, 130.0, 116.9, 112.9, 108.1, 104.7, 61.6, 61.5, 56.8. ESI MS (*m*/*e*) 416.06 $[M+1]^+$. Purity: 95.9% by HPLC.

*4.1.3.8. N-(2-Bromo-3,4,5-trimethoxybenzyl)-5-chloro-2,4-dihydroxy-N-methylbenzamide (**21g**).* 21% yield. R_f = 0.24 (1:1 ethyl acetate: hexane). ^{1}H NMR (500 MHz, CD_3OD) δ 7.15 (s, 1H), 6.92 (s, 1H), 6.49 (s, 1H), 4.70 (s, 2H), 3.82 (s, 6H), 3.81 (s, 3H), 2.96 (s, 3H). ^{13}C NMR (125 MHz, CD_3OD) δ 170.5, 155.2, 153.7, 153.4, 150.9, 142.1, 131.1, 128.7, 115.8, 111.4, 108.4, 106.9, 103.3, 78.1, 60.1, 55.5, 51.2, 36.3. ESI MS (*m*/*e*) 462.01 $[M+1]^+$. Purity: 96.6% by HPLC.

*4.1.3.9. 5-Chloro-2,4-dihydroxy-N-methyl-N-(3-methylbenzyl)benzamide (**21h**).* 90% yield. R_f = 0.23 (1:4 ethyl acetate: hexane). ^{1}H NMR (500 MHz, CD_3OD) δ 7.25 (s, 1H), 7.17–7.15 (m, 4H), 6.50 (s, 1H), 4.66 (s, 2H), 3.56 (s, 3H), 2.30–2.24 (m, 3H). ^{13}C NMR (125 MHz, CD_3OD) δ 171.5, 156.5, 155.4, 137.5, 135.4, 131.4, 130.1, 128.7, 128.5, 127.1, 117.0, 112.5, 104.5, 36.6, 49.8, 19.2. ESI MS (*m*/*e*) 306.08 $[M+1]^+$. Purity: 100.0% by HPLC.

*4.1.4. General procedure for the synthesis of compounds (**23a-b** and **28a**)*

Compound **22** (1 equiv) was added to a benzyl amine derivatives (**12a-b** and **27**) (1.5 equiv), 1-ethyl-3-(3-dimethylaminopropyl) carbodiimide (2 equiv), 1-hydroxybenzotriazole monohydrate (1 equiv) and *N*,*N*-diisopropylethylamine (1 equiv) in DMF. The reaction mixture was stirred under microwave irradiation at 120 °C for 3 h. After completion of the reaction, the mixture was dissolved in ethyl acetate. The organic layer was washed with saturated 1N-HCl three times, dried over Na_2SO_4, concentrated under reduced pressure and purified by HPLC or MPLC to afford compound **23a-b** and **28a** in 26–69% yield.

*4.1.4.1. 5-Chloro-2,4-dihydroxy-N-methyl-N-(3-methylbenzyl)benzamide (**23a**).* 69% yield. R_f = 0.20 (3:7 ethyl acetate: hexane). ^{1}H NMR (500 MHz, CD_3OD) δ 7.21–7.19 (m, 2H), 7.16 (s, 1H), 7.07 (d, *J* = 7.5 Hz, 2H), 6.51 (s, 1H), 4.59 (s, 2H), 2.88 (s, 3H), 2.31 (s, 3H). ^{13}C NMR (125 MHz, CD_3OD) δ 170.3, 155.1, 154.1, 138.2, 136.5, 128.7, 128.3, 128.0, 127.9, 124.4, 115.9, 111.3, 103.7, 52.1, 34.1, 20.2. ESI MS (*m*/*e*) 306.08 $[M+1]^+$. Purity: 97.3% by HPLC.

*4.1.4.2. 5-Chloro-2,4-dihydroxy-N-methyl-N-(4-methylbenzyl)benzamide (**23b**).* 26% yield. R_f = 0.23 (1:4 ethyl acetate: hexane). ^{1}H NMR (500 MHz, CD_3OD) δ 7.15–7.12 (m, 5H), 6.50 (s, 1H), 4.57 (s, 2H), 2.87 (s, 3H), 2.30 (s, 3H). ^{13}C NMR (125 MHz, CD_3OD) δ 170.3, 155.3, 154.2, 137.0, 133.6, 129.0, 128.7, 127.5, 115.7, 111.4, 103.7, 51.9, 33.9, 19.8. ESI MS (*m*/*e*) 306.08 $[M+1]^+$. Purity: 98.9% by HPLC.

*4.1.4.3. Methyl 4-((5-chloro-2,4-dihydroxy-N-methylbenzamido) methyl) benzoate (**28a**).* 76% yield. R_f = 0.15 (2:3 ethyl acetate: hexane). ^{1}H NMR (500 MHz, $CDCl_3$) δ 8.03 (d, *J* = 8.5 Hz, 2H), 7.34 (d,

J = 8.0 Hz, 2H), 7.24 (s, 1H), 6.60 (s, 1H), 4.74 (s, 2H), 3.91 (s, 3H), 3.06 (s, 3H). ^{13}C NMR (125 MHz, $CDCl_3$) δ 171.4, 167.0, 160.0, 155.3, 141.5, 130.4, 129.7, 128.7, 127.5, 110.6, 110.5, 105.2, 52.4, 50.9, 37.1. ESI MS (*m/e*) 350.07 $[M+1]^+$.

*4.1.5. General procedure for the synthesis of compounds (**29a** and **29b**)*

A methyl benzoate derivatives (**28a** and **28b**) (1 equiv) and 20% (w/v) lithium hydroxide in methanol-H_2O (1:1) was stirred at room temperature for 3 h. The mixture was neutralized with 6 N HCl to pH 6 and then extracted with ethyl acetate three times. The organic layer was dried over Na_2SO_4, concentrated under reduced pressure and purified by MPLC (Biotage SNAP HP-Sil column) to afford compound **29a** and **29b** in 85 and 88% yield.

*4.1.5.1. 4-((5-Chloro-2,4-dihydroxy-N-methylbenzamido)methyl) benzoic acid (**29a**).* 85% yield. R_f = 0.19 (1:1 ethyl acetate: hexane). ^{1}H NMR (500 MHz, CD_3OD) δ 8.00 (d, J = 8.0 Hz, 2H), 7.43 (s, 2H), 7.18 (s, 1H), 6.50 (s, 1H), 7.74 (s, 2H), 2.94 (s, 3H). ^{13}C NMR (125 MHz, CD_3OD) δ 171.8, 169.7, 156.5, 155.2, 143.4, 131.1, 130.8, 130.1, 128.5, 117.0, 112.6, 104.6. ESI MS (*m/e*) 336.06 $[M+1]^+$.

*4.1.5.2. 4-((2,4-Dihydroxy-5-isopropyl-N-methylbenzamido)methyl) benzoic acid (**29b**).* 88% yield. R_f = 0.28 (1:1 ethyl acetate: hexane). ^{1}H NMR (500 MHz, CD_3OD) δ 8.00 (d, J = 8.5 Hz, 2H), 7.41 (d, J = 6.5 Hz, 2H), 6.99 (s, 1H), 6.35 (s, 1H), 4.73 (s, 2H), 3.17–3.11 (m, 1H), 2.97 (s, 1H), 1.17–1.11 (m, 6H). ^{13}C NMR (125 MHz, CD_3OD) δ 173.9, 169.6, 158.6, 154.7, 143.9, 131.1, 131.0, 128.4, 128.0, 126.9, 114.6, 103.3, 27.5, 23.0. ESI MS (*m/e*) 344.14 $[M+1]^+$.

*4.1.6. General procedure for preparing bendzamide derivatives (**28b** and **30a-f**)*

The benzoic acid derivatives (**25** and **29a-b)** (1 equiv) was added to a primary alkyl amines (1.5 equiv), 1-ethyl-3-(3-dimethylaminopropyl)carbodiimide (2 equiv), 1-hydroxybenzotriazole monohydrate (1 equiv) and *N*,*N*-diisopropylethylamine (1 equiv) in DMF. The reaction mixture was stirred under microwave irradiation at 120 °C for 3 h. After completion of the reaction, the mixture was dissolved in ethyl acetate. The organic layer was washed with saturated 1N-HCl three times, dried over Na_2SO_4, concentrated under reduced pressure and purified by MPLC to afford compounds **28b** and **30a-f** in 17–82% yield.

*4.1.6.1. Methyl 4-((2,4-dihydroxy-5-isopropyl-N-methylbenzamido)-methyl)benzoate (**28b**).* 82% yield. R_f = 0.13 (3:7 ethyl acetate: hexane). ^{1}H NMR (500 MHz, $CDCl_3$) δ 10.42 (s, 1H), 8.09 (d, J = 8.5 Hz, 2H), 7.39 (d, J = 8.5 Hz, 2H), 7.06 (s,1H), 6.41 (s, 1H), 6.10 (s, 1H), 4.79 (s, 2H), 3.94 (s, 3H), 3.10 (s, 3H), 3.07–3.03 (m, 1H), 0.97 (d, J = 6.5 Hz, 6H). ^{13}C NMR (125 MHz, $CDCl_3$) δ 173.4, 167.0, 159.7, 157.4, 142.2, 130.4, 129.6, 127.1, 126.4, 126.0, 108.8, 104.0, 52.4, 36.7, 26.2, 22.9, 22.6. ESI MS (*m/e*) 358.16 $[M+1]^+$.

*4.1.6.2. 5-Chloro-2,4-dihydroxy-N-methyl-N-(4-(methylcarbamoyl) benzyl)benzamide (**30a**).* 17% yield. R_f = 0.21 (4:1 ethyl acetate: methanol). ^{1}H NMR (500 MHz, $(CD_3)_2SO$) δ 10.36 (s, 1H), 10.11 (s, 1H), 8.43 (dd, J = 8.8 Hz, 4 Hz, 1H), 7.77 (d, J = 8.0, 2H), 7.36 (s, 2H), 7.12 (s, 1H), 6.57 (s, 1H), 4.66 (s, 1H), 2.79–2.77 (m, 6H). ^{13}C NMR (125 MHz, $(CD_3)_2SO$) δ 168.5, 166.9, 154.8, 153.8, 141.0, 133.9, 129.3, 127.8, 127.6, 116.9, 110.5, 104.0, 50.0, 36.3, 26.8. ESI MS (*m/e*) 349.09 $[M+1]^+$. Purity: 99.2% by HPLC.

*4.1.6.3. 5-Chloro-N-(4-(ethylcarbamoyl)benzyl)-2,4-dihydroxy-N-methylbenzamide (**30b**).* 31% yield. R_f = 0.21 (4:1 ethyl acetate: methanol). ^{1}H NMR (500 MHz, $CDCl_3$) δ 7.76 (d, J = 8.0 Hz, 2H), 7.34 (d, J = 8.0 Hz, 2H), 7.25 (s, 1H), 6.66 (s, 1H), 6.11 (s, 1H), 4.74 (s, 2H), 3.53–3.48 (m, 2H), 3.07 (s, 3H), 1.25 (t, J = 7.5 Hz, 3H). ^{13}C NMR (125 MHz, $CDCl_3$) δ 167.2, 160.8, 155.1, 139.8, 134.4, 128.5, 127.8, 127.6, 110.5, 110.1, 110.0, 105.3, 35.1, 15.0. ESI MS (*m/e*) 363.11 $[M+1]^+$. Purity: 95.4% by HPLC.

*4.1.6.4. 5-Chloro-2,4-dihydroxy-N-methyl-N-(4-(propylcarbamoyl) benzyl)benzamide (**30c**).* 46% yield. R_f = 0.21 (7:3 ethyl acetate: methanol). ^{1}H NMR (500 MHz, $(CD_3)_2SO$) δ 10.37 (s, 1H), 10.11 (s, 1H), 8.46 (t, J = 5.5 Hz, 1H), 7.83 (d, J = 8.0 Hz, 2H), 7.38 (s, 2H), 7.13 (s, 1H), 6.59 (s, 1H), 4.67 (s, 2H), 3.21 (t, J = 6.0 Hz, 2H), 2.79 (s, 3H), 1.55–1.48 (m, 2H), 0.87 (t, J = 7.5 Hz, 3H). ^{13}C NMR (125 MHz, $(CD_3)_2SO$) δ 168.6, 166.4, 154.9, 153.9, 141.0, 134.1, 129.4, 127.9, 127.5, 116.9, 110.5, 104.0, 49.9, 41.5, 36.3, 23.0, 12.0. ESI MS (*m/e*) 377.12 $[M+1]^+$. Purity: 95.6% by HPLC.

*4.1.6.5. 2,4-Dihydroxy-5-isopropyl-N-methyl-N-(4-(methyl-carbamoyl)benzyl)-benzamide (**30d**).* 36% yield. R_f = 0.21 (7:3 ethyl acetate: methanol). ^{1}H NMR (500 MHz, $(CD_3)_2SO$) δ 9.66 (s, 1H), 9.53 (s, 1H), 8.43 (d, J = 4.5 Hz, 1H), 7.81 (d, J = 8.0 Hz, 2H), 7.35 (s, 2H), 6.88 (s, 1H), 6.39 (s, 1H), 4.60 (s, 2H), 3.07–3.05 (m, 1H), 2.82 (s, 1H), 2.78 (d, J = 4.0 Hz, 3H), 2.06 (d, J = 2.0 Hz, 6H). ^{13}C NMR (125 MHz, $(CD_3)_2SO$) δ 170.7, 167.0, 156.8, 153.4, 141.3, 134.0, 127.6, 127.5, 126.1, 114.6, 103.0, 51.9, 35.2, 26.7, 26.7, 26.4, 23.1. ESI MS (*m/e*) 357.18 $[M+1]^+$. Purity: 95.4% by HPLC.

*4.1.6.6. N-(4-(Ethylcarbamoyl)benzyl)-2,4-dihydroxy-5-isopropyl-N-methyl-benzamide (**30e**).* 24% yield. R_f = 0.21 (7:3 ethyl acetate: methanol). ^{1}H NMR (500 MHz, $(CD_3)_2SO$) δ 9.61 (s, 1H), 9.49 (s, 1H), 8.42 (t, J = 5.0 Hz, 1H), 7.78 (d, J = 8.0 Hz, 2H), 7.31 (s, 2H), 6.85 (s, 1H), 6.36 (s, 1H), 4.56 (s, 2H), 3.27–3.22 (m, 2H), 3.04–2.99 (m, 1H), 2.78 (s, 3H), 1.07 (t, J = 7.0 Hz, 3H), 1.03 (d, J = 4.0 Hz, 6H). ^{13}C NMR (125 MHz, $(CD_3)_2SO$) δ 170.0, 165.6, 156.1, 152.7, 140.5, 133.5, 127.1, 126.8, 125.4, 113.9, 102.3, 79.0, 51.2, 34.4, 33.9, 25.7, 22.4, 14.6. ESI MS (*m/e*) 357.18 $[M+1]^+$. Purity: 96.6% by HPLC.

*4.1.6.7. 2,4-Dihydroxy-5-isopropyl-N-methyl-N-(4-(propylcarba-moyl)benzyl)-benzamide (**30f**).* 22% yield. R_f = 0.21 (7:3 ethyl acetate: methanol). ^{1}H NMR (500 MHz, (CD_3OD) δ 7.81 (dd, J = 6.3 Hz, 1.5 Hz, 2H), 7.41 (d, J = 5.5 Hz, 2H), 6.99 (s, 1H), 6.35 (s, 1H), 4.72 (s, 2H), 3.33 (t, J = 7.5 Hz, 2H), 3.16–3.13 (m, 1H), 2.96 (s, 3H), 1.66–1.61 (m, 2H), 1.12 (d, J = 7.5 Hz, 6H), 0.97 (t, J = 7.5 Hz, 3H). ^{13}C NMR (125 MHz, CD_3OD) δ 173.9, 169.9, 158.5, 154.6, 142.2, 134.9, 128.6, 128.6, 127.9, 126.9, 114.6, 103.3, 42.8, 24.5, 23.7, 23.1, 11.8. ESI MS (*m/e*) 371.19 $[M+1]^+$. Purity: 95.5% by HPLC.

4.2. Molecular modeling

In silico docking of **21a** or **30f** with the 3D coordinates of the X-ray crystal structures of the N-terminal domain of human Hsp90 (PDB code: 2XJX) was accomplished using the AutoDock program downloaded from the Molecular Graphics Laboratory of the Scripps Research Institute. In the docking experiments carried out, gas-teiger charges were placed on the X-ray structures of the N-terminal domain of Hsp90 along with **21a** or **30f** using tools from the AutoDock suite. A grid box centered on the N-terminal Hsp90 domain with definitions of 60_60_60 points and 0.375 Å spacing was chosen for ligand docking experiments. The docking parameters consisted of setting the population size to 150, the number of generations to 27000, and the number of evaluations to 25000000, while the number of docking runs was set to 100 with a cutoff of 1 Å for the root-mean-square tolerance for the grouping of each docking run. The docking model of human Hsp90 with compound **21a** and **30f** were depicted in Figs. 2 and 4, respectively and rendering of the picture was generated using PyMol (DeLano Scientific).

4.3. Biological activity

4.3.1. Cell culture

Sk-Br3 and H1975 cells were grown in RPMI 1640 (containing 25 mM HEPES) and RPMI 1640 with L-glutamin supplemented with streptomycin (500 mg/mL), penicillin (100 units/mL), and 10% fetal bovine serum (FBS). Cells were grown to confluence in a humidified atmosphere (37 °C, 5% CO_2).

4.3.2. Cell proliferation assay

Cells were seeded at 3000 (Sk-Br3), 1500 (H1975) cells per well in a clear 96-well plate, the medium volume was brought to 100 μL, and the cells were allowed to attach overnight. The next day, varying concentrations of 20, 21a-h, 23a-b (Sk-Br3 and H1975), 30a-f (H1975) or 1% DMSO vehicle control was added to the wells. Cells were then incubated at 37 °C for 1, 2, and 3 days. Cell viability was determined using the Promega Cell Titer 96 Aqueous One Solution cell proliferation assay. After incubation with compounds, 20 μL of the assay substrate solution was added to the wells, and the plate was incubated at 37 °C for an additional 1 h. Absorbance at 490 nm was then read on Tecan Infinite F200 Pro plate reader, and values were expressed as percent of absorbance from cells incubated in DMSO alone.

4.3.3. Western blot

H1975 cells were seeded in 100 mm culture dishes (1×10^6/dish), and allowed to attach overnight. Compound **30f** was added at the concentrations indicated compound (0.05, 0.1, 0.5, and 1 μM) and the cells were incubated for an additional 24 h. For comparison, cells were also incubated with DMSO (1%) or geldanamycin (1 μM) for 24 h. Cells were harvested in ice-cold lysis buffer (23 mM Tris-HCl pH 7.6, 130 mM NaCl, 1% NP-40, 1% sodium deoxycholate, 0.1% SDS), and 30 μg of lysate per lane was separated by SDS-PAGE and followed by transferring to a PVDF membrane (Bio-Rad). The membrane was blocked with 5% skim milk in TBST, and then incubated with the corresponding antibody (EGFR, Her2, Met, Akt, c-Raf, Hsp90, Hsp70, PARP, Caspase 3, Cleaved Caspase 3, Cleaved Caspase 8, Bcl-2, Bax and β-Actin). After binding of an appropriate secondary antibody coupled to horseradish peroxidase, proteins were visualized by ECL chemiluminescence according to the instructions of the manufacturer (GE healthcare, USA).

4.3.4. Fluorescence polarization assay

All fluorescence polarization experiments were conducted in 96 well, black, round-bottom plates using a micro plate reader. For FP assay experiments, to each well was added HFB buffer (20 mM HEPES pH 7.3, 50 mM KCl, 5 mM $MgCl_2$, 20 mM Na_2MoO_4, 0.01% NP-40), 30 nM recombinant Hsp90α full length protein, 5 nM the fluorescein isothiocyanate labeled geldanamycin (GA-FITC) inhibitor, 0.1 mg/mL Bovine globulin (BGG), 2 mM 1,4-dithiothreitol (DTT) and varing concentration of compounds. All wells had a final volume of 100 μL in the HFB buffer. The plate was allowed to incubated at 4 °C for 16 h. The polarization values in millipolarization units (mP) were measured at an excitation wavelength at 495 nm and an emission wavelength at 530 nm. All experimental data were analyzed using Prism software (version 5.0, Graphpad Software, San Diego, CA).

4.3.5. Cytochrome P450 inhibition assay

The inhibitory potency of compound **30f** was determined with cytochrome P450 assays in the absence and presence of compound **30f** (final concentrations of 0–50 μM with acetonitrile concentration less than 0.5%) using pooled human liver microsomes (Xenotech H0630). All experiments were performed in duplicate. Phenacetin *O*-deethylase, tolbutamide 4-hydroxylase, omeprazole hydroxylase, dextromethorphan *O*-demethylase, and midazolam 1′-hydroxylase activities were determined as probe activities for CYP1A2, CYP2C9, CYP2C19, CYP2D6, and CYP3A, respectively, using cocktail incubation and tandem mass spectrometry, as described previously [38,39].

4.3.6. In vivo xenograft

Seven-week-old male NOD-scid IL2Rgamma^{null} (NSG) mice were purchased from Jackson Laboratory (USA) and maintained in accordance with the institutional guidelines of Keimyung University, College of Medicine. All animal studies were carried out according to approved experimental protocols (KM-2016-35). The mice were acclimated for 1 week in individually ventilated cages (IVC) under sterile and standardized environmental conditions (25 ± 2 °C room temperature, 50 ± 10% relative humidity, 12 h light-dark rhythm). H1975 cells (2.0×10^6 cells) were transplanted subcutaneously (s.c.) into the left flank region of mice on experimental day zero. Mice were randomly distributed to the experimental groups (6 mice per group). One week after xenotransplantation, mice were intraperitoneally treated with either compound **30f** (25 mg/kg and 50 mg/kg) or DMSO daily followed by weekend rest for 3 weeks. Tumor size was measured at the time of injection and twice per week afterwards with a caliper in two dimensions. Individual tumor volumes (V) were calculated by formula V= (length × [width]^2)/2.

4.3.7. Immunohistochemistry (IHC)

Mouse tissue was fixed with 10% formalin and embedded in paraffin, and sectioned. The sections were stained with IHC for light microscopic examination. For assessment of Akt staining, 5 μm sections were permeabilized in PBS, incubated in 10 mM sodium citrate buffer with pH 6.0 for 100 °C, 10 min, and the with goat polyclonal anti-Akt (Cat #9272, Cell signaling, USA) antibody. Sections were then incubated with secondary antibody (1:200 dilution, Santa Cruz Biotechnology, USA), followed by staining with diaminobenzidine chromogen (Cat# SK-4105, Vector Laboratories, USA) and counterstaining with hematoxylin (Cat# S3309, Dako, Denmark). The stained sections were examined under microscopy (200) and all histological assessments (Nikon, Japan) were made by a pathologist.

Acknowledgements

This research was supported by Basic Science Research Program through the National Research Foundation of Korea (NRF) funded by the Ministry of Education (NRF-2016R1A6A1A03011325 and 2016R1D1A1B01009559), and by the National Research Foundation of Korea (NRF) grant funded by the Korean Government (MSIP) (No.2014R1A5A2010008).

Appendix A. Supplementary data

Supplementary data related to this article can be found at https://doi.org/10.1016/j.ejmech.2017.11.054.

References

[1] D. Mahalingam, R. Swords, J.S. Carew, S.T. Nawrocki, K. Bhalla, F.J. Giles, Targeting HSP90 for cancer therapy, Br. J. cancer 100 (2009) 1523–1529.
[2] L. Whitesell, S.L. Lindquist, HSP90 and the chaperoning of cancer, Nature reviews, Cancer 5 (2005) 761–772.
[3] J.J. Barrott, T.A. Haystead, Hsp90, an unlikely ally in the war on cancer, FEBS J. 280 (2013) 1381–1396.
[4] K. Esfahani, V. Cohen, HSP90 as a novel molecular target in non-small-cell lung cancer, Lung Cancer (Auckl) 7 (2016) 11–17.
[5] G. Chiosis, L. Neckers, Tumor selectivity of Hsp90 inhibitors: the explanation remains elusive, ACS Chem. Biol. 1 (2006) 279–284.

[6] K. Jhaveri, T. Taldone, S. Modi, G. Chiosis, Advances in the clinical development of heat shock protein 90 (Hsp90) inhibitors in cancers, Biochim. Biophys. Acta 1823 (2012) 742–755.
[7] D.B. Solit, G. Chiosis, Development and application of Hsp90 inhibitors, Drug Discov. today 13 (2008) 38–43.
[8] J. Trepel, M. Mollapour, G. Giaccone, L. Neckers, Targeting the dynamic HSP90 complex in cancer, Nature reviews, Cancer 10 (2010) 537–549.
[9] I. Koca, A. Ozgur, M. Er, M. Gumus, K. Acikalin Coskun, Y. Tutar, Design and synthesis of pyrimidinyl acyl thioureas as novel Hsp90 inhibitors in invasive ductal breast cancer and its bone metastasis, Eur. J. Med. Chem. 122 (2016) 280–290.
[10] C. Liang, H. Hao, X. Wu, Z. Li, J. Zhu, C. Lu, Y. Shen, Design and synthesis of N-(5-chloro-2,4-dihydroxybenzoyl)-(R)-1,2,3,4-tetrahydroisoquinoline-3-carboxamid es as novel Hsp90 inhibitors, Eur. J. Med. Chem. 121 (2016) 272–282.
[11] D. Montoir, S. Barille-Nion, A. Tonnerre, P. Juin, M. Duflos, M.A. Bazin, Novel 1,6-naphthyridin-2(1H)-ones as potential anticancer agents targeting Hsp90, Eur. J. Med. Chem. 119 (2016) 17–33.
[12] L. Wang, L. Li, Z.H. Zhou, Z.Y. Jiang, Q.D. You, X.L. Xu, Structure-based virtual screening and optimization of modulators targeting Hsp90-Cdc37 interaction, Eur. J. Med. Chem. 136 (2017) 63–73.
[13] C. Zhang, X. Wang, H. Liu, M. Zhang, M. Geng, L. Sun, A. Shen, A. Zhang, Design, synthesis and pharmacological evaluation of 4,5-diarylisoxazols bearing amino acid residues within the 3-amido motif as potent heat shock protein 90 (Hsp90) inhibitors, Eur. J. Med. Chem. 125 (2017) 315–326.
[14] L. Whitesell, E.G. Mimnaugh, B. De Costa, C.E. Myers, L.M. Neckers, Inhibition of heat shock protein HSP90-pp60v-src heteroprotein complex formation by benzoquinone ansamycins: essential role for stress proteins in oncogenic transformation, Proc. Natl. Acad. Sci. U. S. A. 91 (1994) 8324–8328.
[15] J.G. Supko, R.L. Hickman, M.R. Grever, L. Malspeis, Preclinical pharmacologic evaluation of geldanamycin as an antitumor agent, Cancer Chemother. Pharmacol. 36 (1995) 305–315.
[16] E. Caldas-Lopes, L. Cerchietti, J.H. Ahn, C.C. Clement, A.I. Robles, A. Rodina, K. Moulick, T. Taldone, A. Gozman, Y. Guo, N. Wu, E. de Stanchina, J. White, S.S. Gross, Y. Ma, L. Varticovski, A. Melnick, G. Chiosis, Hsp90 inhibitor PU-H71, a multimodal inhibitor of malignancy, induces complete responses in triple-negative breast cancer models, Proc. Natl. Acad. Sci. U. S. A. 106 (2009) 8368–8373.
[17] K. Lundgren, H. Zhang, J. Brekken, N. Huser, R.E. Powell, N. Timple, D.J. Busch, L. Neely, J.L. Sensintaffar, Y.C. Yang, A. McKenzie, J. Friedman, R. Scannevin, A. Kamal, K. Hong, S.R. Kasibhatla, M.F. Boehm, F.J. Burrows, BIIB021, an orally available, fully synthetic small-molecule inhibitor of the heat shock protein Hsp90, Mol. Cancer Ther. 8 (2009) 921–929.
[18] R. Bao, C.J. Lai, D.G. Wang, H. Qu, L. Yin, B. Zifcak, X. Tao, J. Wang, R. Atoyan, M. Samson, J. Forrester, G.X. Xu, S. DellaRocca, M. Borek, H.X. Zhai, X. Cai, C. Qian, Targeting heat shock protein 90 with CUDC-305 overcomes erlotinib resistance in non-small cell lung cancer, Mol. Cancer Ther. 8 (2009) 3296–3306.
[19] A.J. Woodhead, H. Angove, M.G. Carr, G. Chessari, M. Congreve, J.E. Coyle, J. Cosme, B. Graham, P.J. Day, R. Downham, L. Fazal, R. Feltell, E. Figueroa, M. Frederickson, J. Lewis, R. McMenamin, C.W. Murray, M.A. O'Brien, L. Parra, S. Patel, T. Phillips, D.C. Rees, S. Rich, D.M. Smith, G. Trewartha, M. Vinkovic, B. Williams, A.J. Woolford, Discovery of (2,4-dihydroxy-5-isopropylphenyl)-[5-(4-methylpiperazin-1-ylmethyl)-1,3-dihydrois oindol-2-yl]methanone (AT13387), a novel inhibitor of the molecular chaperone Hsp90 by fragment based drug design, J. Med. Chem. 53 (2010) 5956–5969.
[20] Y. Wang, J.B. Trepel, L.M. Neckers, G. Giaccone, STA-9090, a small-molecule Hsp90 inhibitor for the potential treatment of cancer, Curr. Opin. Investig. Drugs 11 (2010) 1466–1476.
[21] S.A. Eccles, A. Massey, F.I. Raynaud, S.Y. Sharp, G. Box, M. Valenti, L. Patterson, A. de Haven Brandon, S. Gowan, F. Boxall, W. Aherne, M. Rowlands, A. Hayes, V. Martins, F. Urban, K. Boxall, C. Prodromou, L. Pearl, K. James, T.P. Matthews, K.M. Cheung, A. Kalusa, K. Jones, E. McDonald, X. Barril, P.A. Brough, J.E. Cansfield, B. Dymock, M.J. Drysdale, H. Finch, R. Howes, R.E. Hubbard, A. Surgenor, P. Webb, M. Wood, L. Wright, P. Workman, NVP-AUY922: a novel heat shock protein 90 inhibitor active against xenograft tumor growth, angiogenesis, and metastasis, Cancer Res. 68 (2008) 2850–2860.
[22] S. Ohkubo, Y. Kodama, H. Muraoka, H. Hitotsumachi, C. Yoshimura, M. Kitade, A. Hashimoto, K. Ito, A. Gomori, K. Takahashi, Y. Shibata, A. Kanoh, K. Yonekura, TAS-116, a highly selective inhibitor of heat shock protein 90alpha and beta, demonstrates potent antitumor activity and minimal ocular toxicity in preclinical models, Mol. Cancer Ther. 14 (2015) 14–22.
[23] J. Bussenius, C.M. Blazey, N. Aay, N.K. Anand, A. Arcalas, T. Baik, O.J. Bowles, C.A. Buhr, S. Costanzo, J.K. Curtis, S.C. DeFina, L. Dubenko, T.S. Heuer, P. Huang, C. Jaeger, A. Joshi, A.R. Kennedy, A.I. Kim, K. Lara, J. Lee, J. Li, J.C. Lougheed, S. Ma, S. Malek, J.C. Manalo, J.F. Martini, G. McGrath, M. Nicoll, J.M. Nuss, M. Pack, C.J. Peto, T.H. Tsang, L. Wang, S.W. Womble, M. Yakes, W. Zhang, K.D. Rice, Discovery of XL888: a novel tropane-derived small molecule inhibitor of HSP90, Bioorg Med. Chem. Lett. 22 (2012) 5396–5404.
[24] J.R. Infante, G.J. Weiss, S. Jones, R. Tibes, T.M. Bauer, J.C. Bendell, J.M. Hinson Jr., D.D. Von Hoff, H.A. Burris 3rd, E.O. Orlemans, R.K. Ramanathan, Phase I dose-escalation studies of SNX-5422, an orally bioavailable heat shock protein 90 inhibitor, in patients with refractory solid tumours, Eur. J. Cancer 50 (2014) 2897–2904.
[25] A. Canella, A.M. Welker, J.Y. Yoo, J. Xu, F.S. Abas, D. Kesanakurti, P. Nagarajan, C.E. Beattie, E.P. Sulman, J. Liu, J. Gumin, F.F. Lang, M.N. Gurcan, B. Kaur, D. Sampath, V.K. Puduvalli, Efficacy of onalespib, a long-acting second-generation HSP90 inhibitor, as a single agent and in combination with temozolomide against malignant gliomas, Clin. Cancer Res. 23 (2017) 6215–6226.
[26] S. Chatterjee, T.F. Burns, Targeting heat shock proteins in cancer: a promising therapeutic approach, Int. J. Mol. Sci. 18 (2017). E1978.
[27] S. Chatterjee, E.H. Huang, I. Christie, B.F. Kurland, T.F. Burns, Acquired resistance to the Hsp90 inhibitor, ganetespib, in KRAS-mutant NSCLC is mediated via reactivation of the ERK-p90RSK-mTOR signaling network, Mol. Cancer Ther. 16 (2017) 793–804.
[28] C.H. Jeong, H.B. Park, W.J. Jang, S.H. Jung, Y.H. Seo, Discovery of hybrid Hsp90 inhibitors and their anti-neoplastic effects against gefitinib-resistant non-small cell lung cancer (NSCLC), Bioorg Med. Chem. Lett. 24 (2014) 224–227.
[29] Y.H. Seo, Discovery of 2',4'-dimethoxychalcone as a Hsp90 inhibitor and its effect on iressa-resistant non-small cell lung cancer (NSCLC), Arch. Pharm. Res. 38 (2015) 1783–1788.
[30] Y.H. Seo, Organelle-specific Hsp90 inhibitors, Arch. Pharm. Res. 38 (2015) 1582–1590.
[31] J.H. Jeong, Y.J. Oh, T.K. Kwon, Y.H. Seo, Chalcone-templated Hsp90 inhibitors and their effects on gefitinib resistance in non-small cell lung cancer (NSCLC), Arch. Pharm. Res. 40 (2017) 96–105.
[32] R.F. Bruns, I.A. Watson, Rules for identifying potentially reactive or promiscuous compounds, J. Med. Chem. 55 (2012) 9763–9772.
[33] J.B. Baell, G.A. Holloway, New substructure filters for removal of pan assay interference compounds (PAINS) from screening libraries and for their exclusion in bioassays, J. Med. Chem. 53 (2010) 2719–2740.
[34] P.P. Kung, L. Funk, J. Meng, M. Collins, J.Z. Zhou, M.C. Johnson, A. Ekker, J. Wang, P. Mehta, M.J. Yin, C. Rodgers, J.F. Davies 2nd, E. Bayman, T. Smeal, K.A. Maegley, M.R. Gehring, Dihydroxylphenyl amides as inhibitors of the Hsp90 molecular chaperone, Bioorg Med. Chem. Lett. 18 (2008) 6273–6278.
[35] J.H. Jeong, Y.J. Oh, Y. Lho, S.Y. Park, K.H. Liu, E. Ha, Y.H. Seo, Targeting the entry region of Hsp90's ATP binding pocket with a novel 6,7-dihydrothieno[3,2-c] pyridin-5(4H)-yl amide, Eur. J. Med. Chem. 124 (2016) 1069–1080.
[36] K.D. Freeman-Cook, R.L. Hoffman, T.W. Johnson, Lipophilic efficiency: the most important efficiency metric in medicinal chemistry, Future Med. Chem. 5 (2013) 113–115.
[37] A. Tarcsay, K. Nyiri, G.M. Keseru, Impact of lipophilic efficiency on compound quality, J. Med. Chem. 55 (2012) 1252–1260.
[38] M.J. Kim, H. Kim, I.J. Cha, J.S. Park, J.H. Shon, K.H. Liu, J.G. Shin, High-throughput screening of inhibitory potential of nine cytochrome P450 enzymes in vitro using liquid chromatography/tandem mass spectrometry, Rapid Commun. Mass Spectrom. 19 (2005) 2651–2658.
[39] J.C. Shon, H.S. Shin, Y.K. Seo, Y.R. Yoon, H. Shin, K.H. Liu, Direct infusion MS-based lipid profiling reveals the pharmacological effects of compound K-reinforced ginsenosides in high-fat diet induced obese mice, J. Agric. Food Chem. 63 (2015) 2919–2929.